applied sciences

MDPI

Article

Study of Dynamics in Metallic MEMS Cantilevers—Pull-In Voltage and Actuation Speed

Xiaohui Yang [1,2,*], Philipp Kästner [1], Eireen Käkel [1], Marek Smolarczyk [1], Shujie Liu [1], Qingdang Li [2] and Hartmut Hillmer [1,2]

[1] Institute of Nanostructure Technologies and Analytics (INA), Center for Interdisciplinary Nanostructure Science and Technology (CINSaT), University of Kassel, Heinrich-Plett-Str. 40, 34132 Kassel, Germany
[2] College of Sino-German Institute Science and Technology, Qingdao University of Science and Technology, Qingdao 266061, China
* Correspondence: yang@ina.uni-kassel.de

Abstract: For different metals and varying geometries, this paper presents simulations of electrostatically actuated MEMS cantilevers regarding their influence on pull-in voltage and actuation speed. Three-dimensional electromechanical modeling including many non-linearities has been performed to study some static but mainly dynamic features. The results show that the involved parameters have different influences on the actuation speed and pull-in voltage: lower length, higher thickness as well as lower density and higher Young's modulus of material diminish the actuation time, while longer length, smaller thickness, and smaller Young's modulus reduce the actuation voltages. Shorter actuation times and smaller actuation voltages cannot be obtained and optimized simultaneously. Different metals such as Au, Ag, Cu, Ti, Ni, Al, W, Cr, Ta, and Mo as well as artificial metals are studied and compared. In this study, Al is found to be the best material for achieving shorter actuation times and smaller actuation voltages. The design rules of MEMS cantilevers are derived considering the large variety of studied parameters. Many involved non-linearities are discussed in detail influencing the MEMS dynamics. Finally, the actuation times are related to the existing experimental actuation times of optical MEMS shutters and MEMS cantilevers.

Keywords: MEMS cantilever; pull-in voltage; actuation speed; non-linearity; dynamics; metallic material systems

check for updates

Citation: Yang, X.; Kästner, P.; Käkel, E.; Smolarczyk, M.; Liu, S.; Li, Q.; Hillmer, H. Study of Dynamics in Metallic MEMS Cantilevers—Pull-In Voltage and Actuation Speed. *Appl. Sci.* **2023**, *13*, 1118. https://doi.org/10.3390/app13021118

Academic Editor: Richard Yongqing Fu

Received: 17 November 2022
Revised: 16 December 2022
Accepted: 10 January 2023
Published: 13 January 2023

Copyright: © 2023 by the authors. Licensee MDPI, Basel, Switzerland. This article is an open access article distributed under the terms and conditions of the Creative Commons Attribution (CC BY) license (https://creativecommons.org/licenses/by/4.0/).

1. Introduction

Electrostatically actuated MEMS cantilevers are one of the most typical structures in the field of micro-electromechanical systems (MEMS) and are widely used in many kinds of micro-sensors [1,2], micro-switches [3,4] micro-resonators [5] and many other kinds of micro-actuators [6,7] such as air-bag sensors, particle sensors, mass sensors, optical switches, display subdevices, micro-mirrors, and RF switches because of their simple structure, large actuation force, and for Si-based MEMS, the IC compatibility.

Pull-in voltage and actuation speed are two of the most important properties of electrostatic MEMS cantilevers [8]. For many applications in sensors and switches, lower pull-in voltage reduces the energy consumption, extends the applicable scope, and enhances reliability [9,10]. In MEMS resonators, e.g., the driving voltages need be controlled accurately, and the pull-in phenomenon must be avoided when the devices are working [11]. Higher responsiveness saves operating time and broadens applications, and it is always a huge advantage for all applications. The manufacturing of compact MEMS cantilevers with fast response has been demonstrated via batch manufacturing processes in large quantities at low cost [12]. It has been proven that the dynamic and static pull-in features of cantilevers are affected significantly by small-scale structural and geometric parameters as well as non-linearities [13]. Moreover, higher resonant frequencies and thus faster actuation speed can be achieved as the microstructures become smaller [14].

All these points define research gaps and a strong motivation to identify contributions to design rules leading to improvements in MEMS dynamics regarding pull-in voltage and actuation speed.

Many studies and simulations on MEMS cantilevers have been reported. Siddaiah et al. presented a U-shaped and rectangular triple-coupled micro-cantilever and simulated corresponding eigenfrequencies, surface stresses and displacements. The results showed that the U-shaped structure reveals higher sensitivity than the rectangular one [15]. Tuma and Skutova calculated the transfer function relating the displacement to the acting force and simulated the time response following an acting force [16]. Sanchez-Fraga et al. designed a mass sensor based on a silicon MEMS cantilever which is horizontally actuable and simulated eigenfrequency and displacement under voltage of the sensor with and without added mass [17]. Xu et al. investigated and optimized MEMS cantilevers based on the simulation results of vibration modes, effect of slots and effect of edge serration [18]. Arya et al. designed and fabricated an electrostatically actuable cantilever arrays as an audible frequency generator and simulated the vibration response under pulsed signal input [19]. In the study of uniaxial capacitive accelerometers, Zega et al. simulated the frequencies of combs of cantilevers. The results have good agreements when a reduced thickness is considered [20]. Sharma et.al proposed an analytical model for static and dynamic pull-in of curled microcantilevers and found an excellent agreement of the present results [21].

Silicon is the by far dominating MEMS material. However, there are also metallic materials in use for specific MEMS devices, such as optical MEMS shutter arrays for smart glass applications [22–31] to modulate daylight in windows, for space instrumentation [28], for camera shutters [32], and for artificial eyelids for sensor protection [33] and displays [22–24,30,34,35]. In the anchor region, these MEMS shutters are fixed to the transparent conductive oxide layer located on the glass substrate. Due to intrinsic stress, these shutter blades are curled in the open state and are uncurled by electrostatic actuation to close them toward the glass substrate. For active daylight steering applications, our flat metallic micromirrors [25,26] have been developed, which are flat in the mirror region by stress compensation. These metallic MEMS mirror actuators have an anchor region, a curled hinge region, and a flat mirror region.

For all these metallic and hybrid MEMS shutter and micro-mirror arrays for optical applications [22–35], the closing time or the actuation time is crucial. Since the shutter dynamics is also related to the magnitude of the applied voltage, also the pull-in voltage is involved and of high interest. Therefore, the main motivation of our paper is to simulate how pull-in voltage and actuation speed depend on geometrical shape and metallic material parameters and to provide support in material selection and optimization. Our studies are contributing to design rules by identifying the trends, in which way dynamic properties depend on different metallic materials, geometrical shapes and material parameters. The knowledge of these trends is helpful in the design process of electrostatic MEMS actuators. Our studies further reveal that expensive materials can be avoided in the design of metallic MEMS devices since low-cost materials deliver even better performance.

The structure of this paper is given in the following. First, the pull-in voltage and actuation time of electrostatically actuated metallic MEMS cantilevers are studied as a function of geometrical and material parameters. This will be completed twice, analytically and numerically. For simple idealized parallel plate MEMS actuators, an analytical formula can be given for the pull-in voltage (in Section 2) and for the eigenfrequency, charging time and the temporal step-response function (in Section 3). Basic knowledge is recalled in Sections 2 and 3 as well as reconsidered in Section 4 for qualitative explanation of the numerical simulation results. The analytical formulas displayed below in Sections 2 and 3 are intended to simplify the access to Section 4 and to support a better intuitive understanding of the MEMS cantilever device studied in Section 4. For the latter device, no analytical formulas are given. In Section 4, COMSOL Multiphysics is used for numerical simulations based on a self-consistent solution of electro-mechanical equations concerning all these properties. but with the focus on pull-in voltage and actuation speed for different metals

and varying geometries. In Section 5, the results of Section 4 are compared with trends from analytical formula: in Section 5.1 for a parallel plate MEMS actuator and in Section 5.2 for a cantilever MEMS actuator. Section 6 proposes the workflow of optimization processes.

2. Idealized Parallel Plate MEMS Actuator: Introduction of the Pull-In Effect

2.1. Model and Differential Equation

First, the 2D schematic of an idealized parallel plate actuator is shown in Figure 1. This is a spring–mass–damper system and represents a typical second-order system. The initial gap distance between two electrodes is described by d.

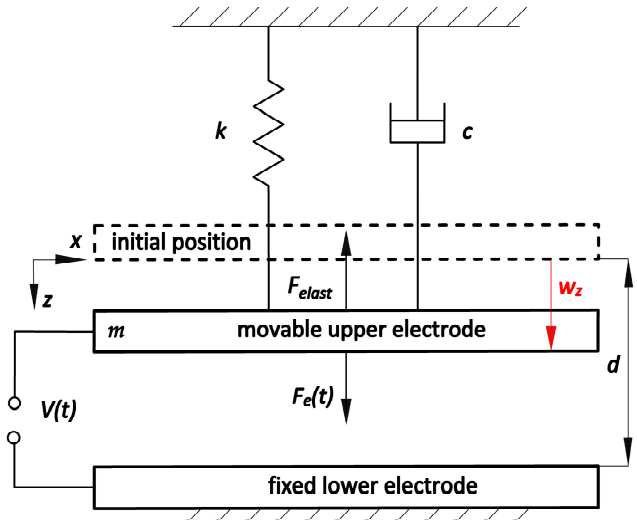


Figure 1. A 2D schematic of a parallel plate MEMS capacitor. A static situation is depicted here, where the elastic restoring force is in equilibrium with the external electrostatic force.

The static and dynamic properties of this idealized oscillator structure can be characterized by a differential equation describing that the sum of the inertia force, the friction force and the elastic restoring force is equal to the external force (here the electrostatic actuation force):

$$m\ddot{w}_z(t) + c\dot{w}_z(t) + kw_z(t) = F_e(t) \tag{1}$$

where m, $wz(t)$, $\dot{w}z(t)$ and $\ddot{w}z(t)$ represent the mass, position, velocity and acceleration, respectively. The spring constant k is an inherent material property of the spring which represents the tendency to return to the initial state when the cantilever is subjected for a moment to an external excitation force $F_e(t)$. The damping coefficient c represents the characteristic that the vibration amplitude gradually decreases due to inherent or external friction. If an external voltage V is applied, the movable electrode will be pulled down by the electrostatic force $F_e(t)$ [36]:

$$F_e(t) = \frac{\varepsilon A V^2(t)}{2(d - w_z(t))^2} \tag{2}$$

where ε is the dielectric constant of the surrounding medium, A is the area of the plate and d is the initial distance between the two electrodes. Dynamic variables are the displacement $w_z(t)$ of the movable plate and the applied voltage $V(t)$. Equation (2) shows a nonlinear relation between $F_e(t)$ and $w_z(t)$. Here, the elastic force $F_{elast}(t) = kw_z(t)$ reveals a linear dependence on the displacement $w_z(t)$. A schematic of the elastic force and the electrostatic actuation force is shown in Figure 2.

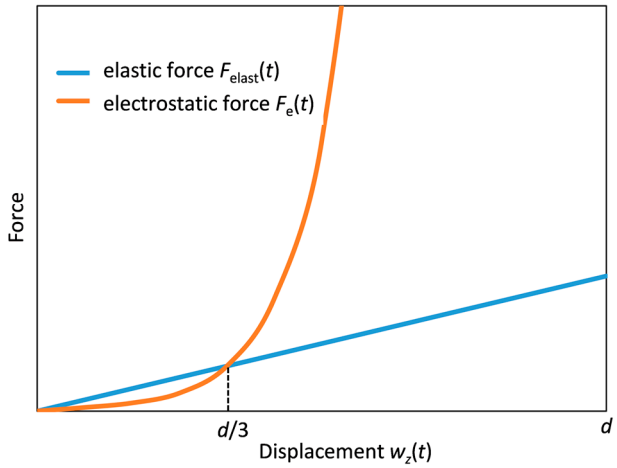


Figure 2. Schematic of forces as a function of displacement.

2.2. Pull-In Voltage

During the continuous process in which the upper electrode is moving toward the lower electrode, it will suddenly snap down to the fixed capacitor when the voltage increases to a threshold value, which is named the pull-in voltage. For a quasi-static condition ($\dot{w}z(t) = \ddot{w}z(t) = 0$), the required voltage V_s for a particular equilibrium position combining Equations (1) and (2) can be written as:

$$Vs = \sqrt{\frac{2kw_z(t)\cdot[d - w_z(t)]^2}{\varepsilon A}} \tag{3}$$

The V_s has a maximum value when $w_z(t) = d/3$ and when the voltage continues to increase, the electrostatic force grows much faster than the spring force, no force equilibrium is possible anymore, and therefore, the pull-in (snap-down) occurs. The value of quasi-static pull-in voltage V_{pi} is:

$$Vpi = \sqrt{\frac{8kd^3}{27\varepsilon A}} \tag{4}$$

3. Dynamic Properties of the Idealized Parallel Plate MEMS Actuator

In practical applications, the input signal for a MEMS actuator is normally a dynamic value such as sinusoidal functions, cosine functions, step-function and so on. In addition, here, we recall some basic knowledge, briefly. The analytical formula displayed below describe an idealized parallel plate MEMS actuator as shown in Section 2. Note that this section is intended to support the understanding of the MEMS cantilever actuators (in Section 4) for which no analytical formula is given.

3.1. Eigenfrequency

Without external excitation force $F_e(t)$, the device oscillates at the eigenfrequency (also called resonance frequency or natural frequency) [37]:

$$f_n = \frac{1}{2\pi}\sqrt{\frac{k}{m}} \tag{5}$$

$$f_d = f_n\sqrt{1 - \zeta^2} \tag{6}$$

with

$$\zeta = \frac{c}{4\pi m f_n} \tag{7}$$

where f_n is the eigenfrequency without damping and f_d is the eigenfrequency of order n with damping. ζ is the damping ratio, which is a dimensionless measure describing how oscillations in a system decay after external excitation is switched off. When $\zeta = 0$, $0 < \zeta < 1$, $\zeta = 1$ and $\zeta > 1$, these systems are called an undamped system, underdamped system, critical damped system and overdamped system, respectively. The eigenfrequency f_n is affected by geometrical and material parameters. Oscillations with larger amplitudes appear in the system when the frequency of input signal is close to the eigenfrequency.

3.2. Step Response

For many MEMS actuators, a common input signal is a temporal voltage step-function. For an underdamped second-order system, the corresponding step response of a real parallel plate MEMS actuator is shown in Figure 3. The response curve reaches a first extremum at the time t_v and after further damped oscillations tends to a steady-state value. The system overshoots the equilibrium position temporally, which means the movable plate has a larger displacement there than for the static value. In this case, temporally, the electrostatic force becomes greater and might reduce the pull-in voltage. This dynamic pull-in voltage is represented by V_{pi}'.

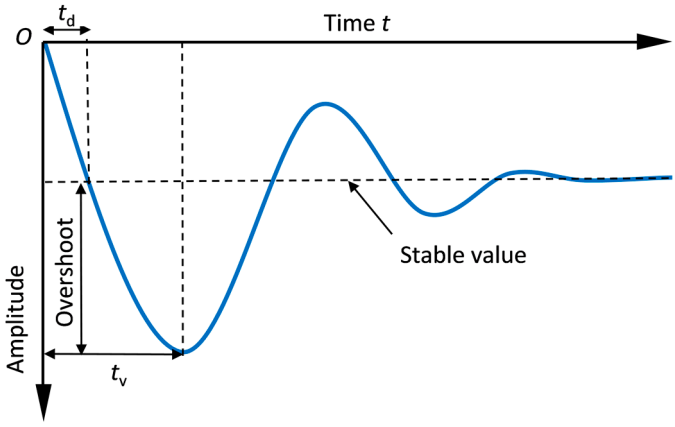


Figure 3. Performance of the step response for a second-order system (completely redrawn using the idea of [37]).

The swiftness of the step response is described by the characteristic times t_d and t_v, which are defined in Figure 3 given by [37]:

$$t_d = \frac{\pi - \beta}{2\pi f_n \sqrt{1-\zeta^2}} \tag{8}$$

$$t_v = \frac{1}{2 f_n \sqrt{1-\zeta^2}} \tag{9}$$

$$\beta = \arctan \frac{\sqrt{1-\zeta^2}}{\zeta} \tag{10}$$

where β is the phase angle of this system. As f_n increases and ζ decreases, t_d and t_v decrease, which means the system has a faster response speed which is related to geometrical and material parameters.

4. Metallic MEMS Cantilevers: Nonlinear Dynamics of the Pull-In Behavior

The goal of our paper is to study the nonlinear dynamics of the pull-in effect of metallic MEMS cantilevers as a function of different cantilever geometries (thickness, length) and material parameters (mass density, Young's modulus). This section presents the influence of different parameters on the pull-in voltage and actuation speed of the MEMS cantilevers,

which are made of different metals. At the beginning of Section 4, a distinct separation of Sections 2 and 3 versus Section 4 is prepended.

In Sections 2 and 3, an idealized parallel plate actuator is considered:

- It is a 1D problem.
- An idealized spiral spring is considered, revealing a linear stress–strain relation (Hooke's law, i.e., linear force–displacement relation).
- The electrostatic force depends on the square of the displacement and the problem can be treated on the basis of analytical formula.

In Section 4, a metallic MEMS cantilever is considered:

- It is a more complex 3D problem.
- The electrical field is varying in 3D, i.e., it is a 3D vector field. Close to the surfaces of the electrodes, the electrical field is perpendicular to the surfaces. The local electrostatic forces vary with x, y and z.
- The electrical capacity is varying with the voltage in a nonlinear way. Thus, also the charging of the cantilever/base plate cannot be any longer treated as a simple RC element. The voltage built up at the MEMS cantilever is not any more simply exponential.
- A non-homogenous charge distribution is existing, and it is varying dynamically.
- The description of the elastic behavior is 3D and based on continuum mechanics.
- Stray fields in the y-direction and x-direction are considered.
- Nearly all relations are nonlinear.
- The problem has to be treated by a self-consistent dynamic electro-mechanical numerical model. COMSOL Multiphysics is used here.

First, a 3D representation of the considered MEMS cantilevers is shown in Figure 4. The metallic cantilever is characterized by the length l, thickness h, width b, mass density ρ and Young's modulus E. In Figure 5, a 2D cross-section of the cantilever taken in the center of the width b in the xz-plane is shown, including electrical field lines (blue) and electrostatic forces (red), schematically. The density of the field lines indicates the magnitude of the electrical field. The stray fields in the x-direction are shown at the right-hand side end of the cantilever. The electrostatic forces are always oriented in the direction of a tangent to the field lines. Thus, the force increases with growing x at the lower surface of the cantilever (upper electrode) and is oriented vertical to the surface, locally. As a consequence of the bending, the electrical capacitance of the system nonlinearly increases as the voltage increases.

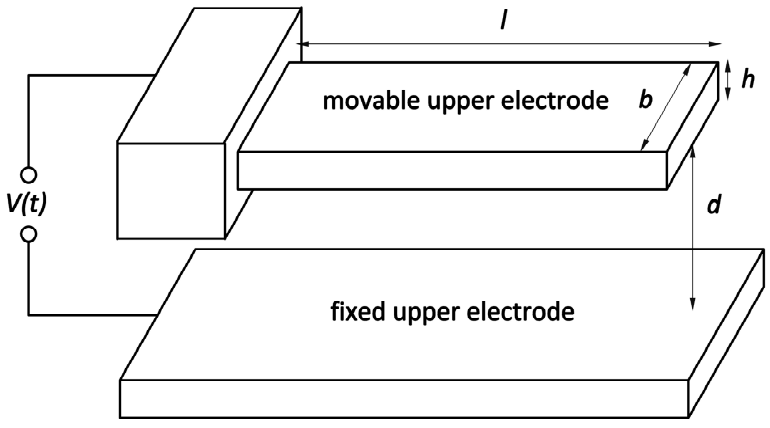


Figure 4. Simulation model of electrostatic MEMS cantilever.

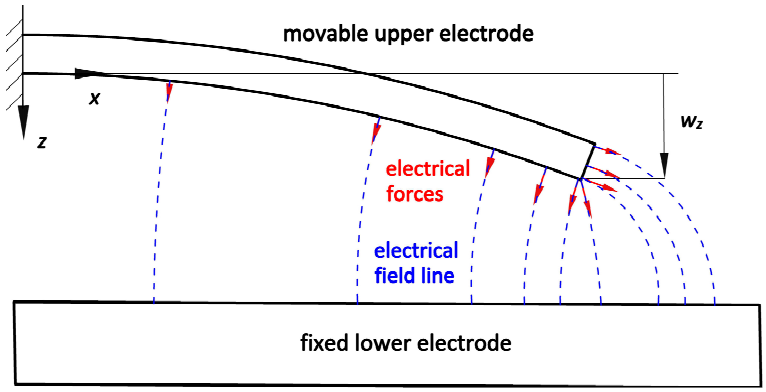


Figure 5. Schematic 2D cross-section of an electrostatically actuated cantilever, displaying the electric field lines (blue) and the electrostatic force (red) in *xz*-space.

COMSOL Multiphysics® 5.6 is a simulation tool with Multiphysics field coupling including a MEMS module that can be used for the simulations on a microscopic scale. As the cantilever bends, the air gap geometry changes as a function of coordinates and leads to local changes in the electric field between the two electrodes, together with the varying charge distribution. The electrostatic field in the air gap is described by Poisson's equation. The coupled physics is handled self-consistently by the Electromechanics Multiphysics modules. The electrostatic force density that acts on the electrode of the cantilever is simulated by COMSOL [38]:

$$\boldsymbol{F_{es}} = -\frac{1}{2}(\boldsymbol{E}\cdot\boldsymbol{D})\boldsymbol{n} + (\boldsymbol{n}\cdot\boldsymbol{E})\boldsymbol{D} \tag{11}$$

where $\boldsymbol{E}$ and $\boldsymbol{D}$ are the electric field and electric flux density vector fields, respectively, and $\boldsymbol{n}$ is the outward normal vector of the surface. This force is always oriented along the normal of the boundary. So, COMSOL can self-consistently handle variations with changing vector field directions and varying parameter values. The problem of displacement is treated using continuum mechanics involving the strain tensor, stress tensor, and elasticity tensor.

In this paper, the stress–strain relation is considered to be linear. This a valid approximation if the displacements are small related to the total length of the cantilever. The extension of the linear stress–strain regime is strongly dependent on the metal materials: highly elastic materials such as steel show a large one, and ductile materials such as copper show a small one. Beyond the linear regime, all materials show nonlinear behavior.

Rayleigh damping has been considered, keeping the coefficients constant (mass damping parameter α_{dM} and stiffness damping parameter β_{dK}) for the dynamic studies. As mentioned by COMSOL for many applications, it is common to assume the case of damping being proportional to the stiffness, and it is sufficient in that case to consider $\alpha_{\mathrm{dM}} = 0$ and to define damping only using the coefficient $\beta_{\mathrm{dK}} = \eta/2\pi f$ [39]. The loss factor η of aluminum at a given frequency $f = 80$ kHz is 0.05% [40]. This provides the two values $\alpha_{\mathrm{dM}} = 0$ and $\beta_{\mathrm{dK}} = 1 \times 10^{-9}$ s. As already mentioned, we kept damping constant, since variable damping was not the scope of our paper. Damping has been found to have a major influence on the dynamics of MEMS devices and has been studied in detail in [41], revealing excellent insights on this crucial point.

In the following, 3D electro-mechanical simulations of MEMS cantilever (as defined in Figures 4 and 5) are performed for different geometrical and material parameters compiled in Table 1. For the meshing of the model, tetrahedra, triangles, edge elements and vertex elements have been automatically built by COMSOL.

Table 1. Geometrical and material parameters of the considered metallic MEMS cantilevers.

Parameters	Values
Length (l)	50–400 µm
Thickness (h)	1–2 µm
Width (b)	20 µm
Air gap distance (d)	3 µm
Young's modulus (E)	35–411 GPa
Mass density (ρ)	2700–19,350 kg/m^3
Poisson ratio (v)	0.21–0.44
Specific electrical resistivity (ρ_R)	1.587–42 $\times$ 10^{-8} Ω·m

Regarding E-ρ charts of materials [42], foams, natural materials, polymers, elastomers, technical ceramics, composites and metals can be found in characteristic "bubbles". For some selected metals, we depict an orange "bubble" in Figure 6. The red rectangles represent the metal materials used in our simulations, and the white rectangles show further metals for comparison. To identify the influence of different values for ρ and E, separately and together, artificial metals not existing in nature are also considered (red points in Figure 6). These ρ and E variations are starting from aluminum (Al) as a reference and are displayed by black arrows.

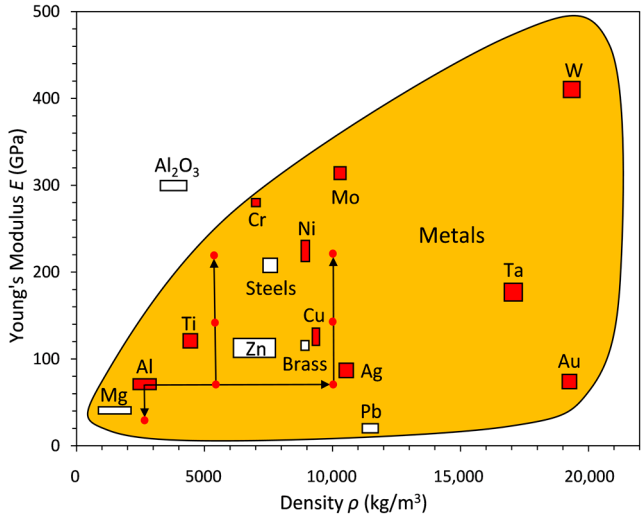


Figure 6. Young's modulus density chart for different metals (completely redrawn using ideas of Reference A [42]).

4.1. Simulation of Pull-In Voltages and Displacements for Electrostatic Actuations

First, stationary simulations are performed for increasing applied voltages. In the voltage–displacement relations, the increase in voltage is interrupted when the pull-in is reached (pull-in voltage V_{pi}). In Figure 7, the displacement–voltage curve for an Al MEMS cantilever with l = 100 µm, h = 1 µm, ρ = 2700 kg/m^3 and E = 70 GPa is shown. As above, the displacement w_z of the cantilever tip is considered in the z-direction. The simulation stops when the voltage approaches 24.41 V and some irregular variations occur (magnified curve area shown in the inset). However, finally, the cantilever free end (tip) reveals a sudden strong displacement through the entire gap, leading to a contact of the cantilever tip to the lower electrode (snap-down). Beyond the pull-in point A, the elastic counterforces are no longer able to balance the electrostatic attraction forces. Therefore, we define the pull-in voltage V_{pi} by the voltage value at the end of the curve still allowing force equilibria between attraction and repulsion before the abrupt change into the non-equilibrium condition occurs.

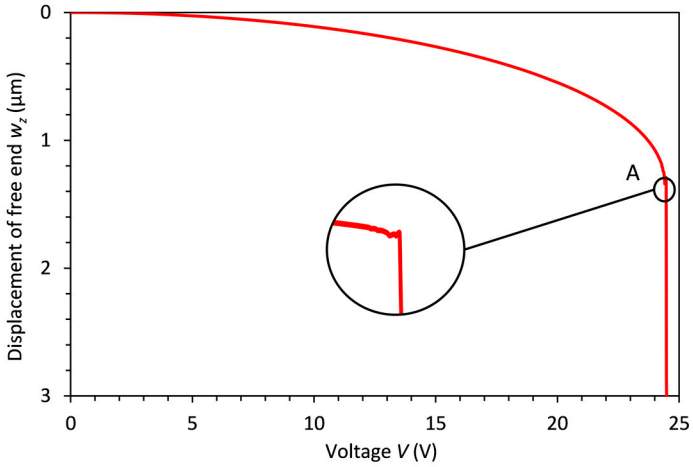


Figure 7. Displacement of the free end (tip) of an Al cantilever as a function of voltage.

In order to study the influences of several parameters on V_{pi}, four groups with varying l, h, ρ and E are considered. The pull-in voltages V_{pi} and the corresponding pull-in displacements w_{pi} of the four groups are shown in Table 2. Group 1 and 2 are considering Al MEMS cantilevers with h = 1 µm and h = 2 µm, respectively. Group 3 considers a halved value of E (35 MPa) compared to Al (left, vertical downward-pointing arrow in Figure 6). Group 4 considers a doubled value of ρ (5400 kg/m^3) compared to Al (left point of the horizontal arrow in Figure 6). The results illustrate that the V_{pi} values are significantly different, but the w_{pi} values remain close to each other, which means l, h and E have a huge influence on V_{pi} but little impact on w_{pi}. In addition, comparing the results of Group 1 and 4, ρ has no significant effect on V_{pi}. The mean values of w_{pi} of three groups are 1.34 µm, 1.36 µm, 1.34 µm and 1.30 µm, which translate to 44.7%, 45.3%, 44.7% and 43.3% of the d, respectively. It indicates that there is only a very weak relationship between the w_{pi} and these parameters of the cantilever.

Table 2. Pull-in voltages V_{pi} and displacements w_{pi} of cantilevers for different l, h, E and ρ.

***l*/µm**	**50**	**100**	**200**	**300**	**400**
Group 1: h = 1 µm, E = 70 GPa, ρ = 2700 kg/m^3 (Al cantilever)					
V_{pi}/V	99.66	24.41	6.28	2.74	1.53
w_{pi} /µm	1.37	1.34	1.36	1.31	1.31
Group 2: h = 2 µm, E = 70 GPa, ρ = 2700 kg/m^3 (Al cantilever)					
V_{pi}/V	291.21	71.02	17.54	7.82	4.30
w_{pi} /µm	1.32	1.36	1.35	1.36	1.39
Group 3: h = 1 µm, E = 35 GPa, ρ = 2700 kg/m^3 (Cantilevers with half E of Al)					
V_{pi}/V	70	17.26	4.44	1.94	1.08
w_{pi}/µm	1.34	1.34	1.36	1.36	1.30
Group 4: h = 1 µm, E = 70 GPa, ρ = 5400 kg/m^3(Cantilevers with double ρ of Al)					
V_{pi} /V	99.03	23.84	6.25	2.71	1.54
w_{pi} /µm	1.34	1.30	1.36	1.23	1.26

Based on the data from these groups of Table 2, further displacement curves of the free ends as a function of voltage are shown in Figure 8 in order to illustrate the influence of different parameters on the V_{pi}. The Al MEMS cantilever with parameters l = 100 µm, h = 1 µm, and E = 70 GPa (case 1 in blue color) is set to a reference. Within each group, we have different cases. Based on the structure of case 1, case 2 with doubled h = 2 µm,

case 3 with halved E = 35 GPa and case 4 with halved l = 50 µm are represented by green, orange and purple curves, respectively. The pull-in voltage of the reference case is named V_{pi1} and the three cases are described by V_{pi2}, V_{pi3} and V_{pi4}. The V_{pi1} value is 1.41 times that of V_{pi3}, while the V_{pi2} and V_{pi4} values are 2.91 and 4.08 times that of V_{pi1}. Thus, it is demonstrated that the degree of influence of these parameters on the V_{pi} is in descending order in the sequence of l, h, and E.

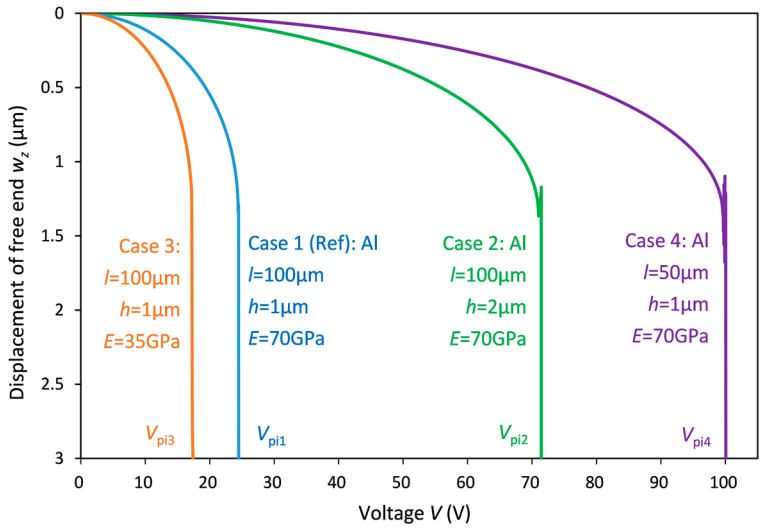


Figure 8. Displacement of the cantilever tip as a function of voltage for different MEMS cantilevers, keeping ρ = 2700 kg/m^3 constant. These colors correspond to the colors in Table 2.

In Figure 6, outside of the orange metal "bubble", the properties of Al_2O_3 are also shown. Even when Al is only shortly exposed to oxygen or water, a thin natural oxide layer of about 4 nm thickness is growing on the Al surfaces. This oxide layer is sealing the underneath pure metal and is not revealing ongoing oxidization if no artificial anodization (eloxal) processes are applied. Al_2O_3 belongs to the "bubble" of the dielectric materials [42]. We checked that the existence of the natural oxide is influencing our pull-in voltage only by 3.8%. We compared the pull-in voltage for a pure Al cantilever with h = 1000 nm thickness with an Al cantilever with natural oxides having the same total thickness h = (4 + 992 + 4) nm.

4.2. Simulation of Resonance Frequencies

First, we will recall and demonstrate that the actuation speed of MEMS cantilevers is related to the mechanical oscillation modes and their corresponding resonance frequencies f_{n} (mechanical Eigenfrequencies or natural frequencies). Each characteristic dynamic movement of the cantilever can be attributed to one or a superposition of several modes (There are different notations in the literature for the resonance frequencies (eigenfrequencies, natural frequencies). In some cases in the literature, the notation is as follows: fundamental mode, 1st order mode, 2nd order mode, 3rd order mode.To make it as simple as possible for the reader, we use the following notation instead: 1st order mode, 2nd order mode, 3rd order mode, 4th order mode. These modes are also related to mechanical eigenfunctions, and the corresponding mechanical resonance frequencies are also called eigenvalues). The cantilever movement which has been considered up to now is simple and is representing the fundamental mode (here, we call it the 1st order mode, which is characterized by the resonance frequency f_1). The higher f_1, the faster the response speed (e.g., shorter actuation time until the cantilever tip has reached the lower electrode). In general, the higher f_{n}, the faster the response speed of motions in that characteristic way.

For the Al cantilever with l = 100 µm, h = 1 µm, b = 20 µm, E = 70 GPa and ρ = 2700 kg/m^3, the 1st order, 2nd order, 3rd order, and 4th order eigenfrequencies as

well as the mode shapes (Eigenfunctions) are shown in Figure 9. The 1st order mode shape is the fundamental bending oscillation with a frequency of 83.87 kHz. Here, the tip oscillates the strongest. The 2nd order mode shape has one node line and is oscillating in the middle and oscillating in the opposite direction at the free-end (tip), and the eigenfrequency equals 525 kHz. The 3rd order mode shape is the torsion motion, and the eigenfrequency is 810 kHz. The 4th order mode shape has three oscillation ranges and two node lines, and it comes with an eigenfrequency of 1470 kHz.

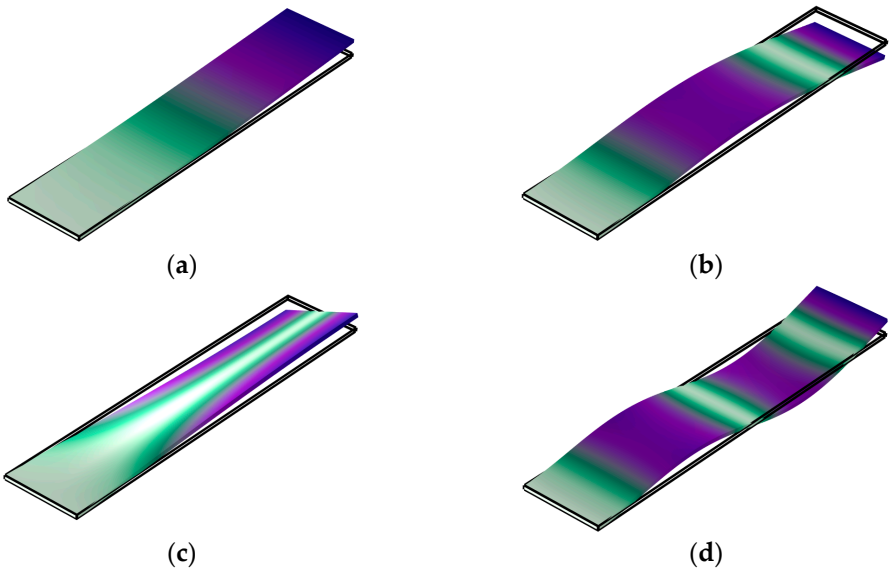


Figure 9. The eigenfunctions of the lowest four modes having the lowest eigenfrequencies: (**a**) 1st order mode, (**b**) 2nd order mode, (**c**) 3rd order mode, (**d**) 4th order mode.

The operating modus of the MEMS cantilever considered here is related to the 1st order mode having no node outside of the fixed end. At the tip (free-end), the cantilever is always most displaced, as already mentioned. Among the lowest four modes, only the first mode shape contributes to the pull-in process, so this mode is normally used to actuate the cantilever and to study its time response.

4.3. Simulation of Dynamic Properties

The required time to reach a certain final situation after the electrostatic actuation of the MEMS cantilevers includes two aspects: the temporal charging of the electrodes t_c and the mechanical response time t_{mr}.

A simple calculation of the electrical charging time of an Al cantilever with l = 100 µm, b = 20 µm and h = 1 µm which was kept static in a first step (capacitance kept constant) reveals charging times in the fs range. In the next step, the cantilever was slowly actuated, which is leading to a variation of the capacitance. This actuation was performed via a quasi-static variation of the voltages. A corresponding rise in capacitance from 8.6 to only 10.5 fF was observed (Figure 10a). In the third step of fast actuation, the charging time is found to increase but still remains in the fs range. That means that t_c can be neglected, since it is very short compared to t_{mr}.

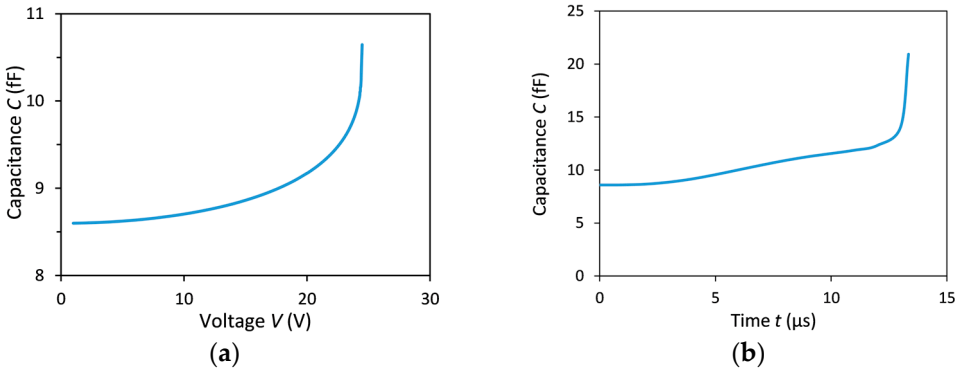


Figure 10. (**a**) Capacitance as a function of actuation voltage, revealing nonlinear rising. (**b**) Capacitance as a function of time, also revealing nonlinear rising. A voltage step function is considered, with a step from zero to 22.2 V occurring at $t = 0$. The simulation includes temporally rising voltage as well as the bending dynamics of the cantilever.

Next, a moving cantilever under a step function of voltage 22.2 V is considered, and the temporal variation of capacitance is simulated by COMSOL and found to be nonlinear (Figure 10b). Due to the temporal bending of the cantilever, the capacitance is varying with the voltage in a nonlinear way. The required time to reach a certain final situation is denoted t_a (actuation time). In our case, the final situation is specified that the tip is reaching the lower electrode (snap-down and pull-in is finished).

Next, the dynamic behavior, i.e., the temporal response curves of this Al MEMS cantilever after applying a step-function at $t = 0$, is simulated. For voltages steps ranging from 22 to 23 V, the results are shown in Figures 11 and 12. The slopes of the curves represent the movement speed of the cantilever tips. Finally, when the voltage is less than or equal to 22.195 V, the system reveals a damped oscillation tending to a stable state. However, when the voltage is higher than 22.196 V, the free-end will snap down and will be attached to the lower electrode. Here, the value of dynamic pull-in voltage is between about 22.196 and 23.0 V and can be represented by V_{pi}', which is smaller than the static pull-in voltage V_{pi} with a value of 24.41 V (shown in Table 2). The reason is that when the displacement w_z is inside the overshoot (see Figure 3) of the step response, the voltage required to generate the same electrostatic force decreases.

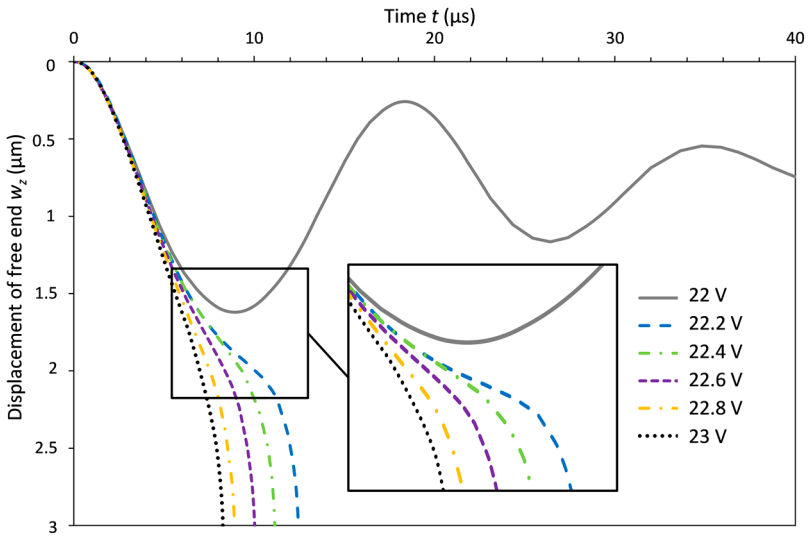


Figure 11. Temporal response of the Al MEMS cantilever tip for different applied voltages; l = 100 μm, b = 20 μm and h = 1 μm.

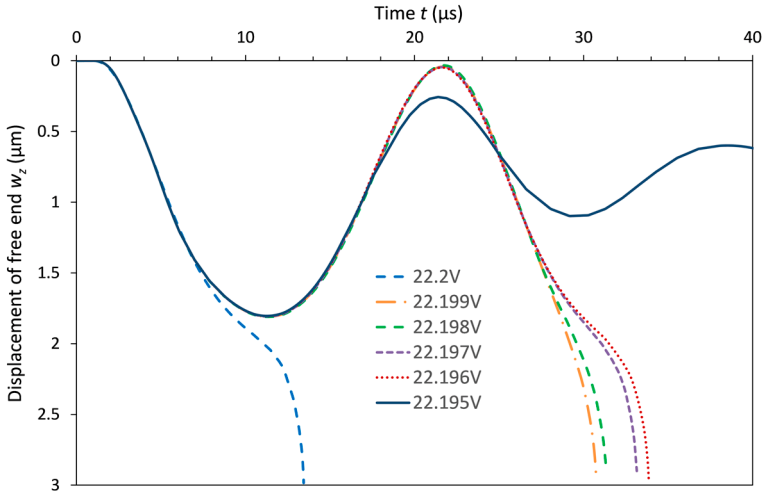


Figure 12. Additional temporal response curves of the same Al MEMS cantilever tip for different applied voltages.

The inset of Figure 11 indicates that when the applied voltage is at 22.2 V, the movements show retardation effects in the pull-in process. At the beginning, the free-end acts fast, a bit later, the moving speed slows down, and finally, the pull-in is completed by a rapid motion. In the meantime, as the voltage increases, the time required for the pull-in to occur becomes shorter, and the retardation effects become weaker. This is because the cantilevers always tend to oscillate, and as the w_z approaches the peak value of oscillation, the velocity of the free-end decreases, while the w_z still raises, causing a continuous increase in the F_e. When the cantilever tip passes the critical point, the increasing speed of F_e is faster than for F_{elast}, so the pull-in action completes quickly.

Similar studies have been reported in Ref [43], focusing on transition to a chaotic behavior for specific voltages. Different authors use different wordings such as chaos, irregularities and instabilities [43,44]. It seems that we can also confirm these findings in a voltage range between 22.199 and 22.2 V for the considered Al cantilever. However, this is not the scope of our paper.

In Figure 12, the retardation is even more pronounced. For voltages between 22.196 and 22.199 V, the pull-in occurs much later after following another oscillation period. Most probably, the pull-in is initiated by a larger peak value at about 22 µs compared to the case at 22.2 V, revealing an ongoing damped oscillation.

Based on the temporal response of an Al MEMS cantilever with a longer length l = 400 µm, Figure 13 shows the retardation effects in a more pronounced way. In this case, the pull-in voltages are smaller than in the previous figures, but when there is a small change in the voltage, the actuation time of cantilever shifts considerably. As the value of voltage changes from 1.4065 to 1.41 V, the actuation time difference is about 60 µs.

Next, for the Al MEMS cantilevers with the parameters E = 70 GPa, ρ = 2700 kg/m^3, h = 1–2 µm, and l = 50–400 µm, the influence of length l and thickness h on actuation time t_a are shown in Figure 14. The actuation time t_a decreases as l decreases and h increases. Among these three points A (h = 1 µm, l = 400 µm), B (h = 1 µm, l = 200 µm) and C (h = 2 µm, l = 400 µm), the point A has the highest actuation time t_{aA}. From point A to B, the length is halved and the actuation time decreases by 75%, and from point A to C, the thickness is doubled and the actuation time reduces by 44%. Thus, the length l has a greater impact on actuation time than the thickness h.

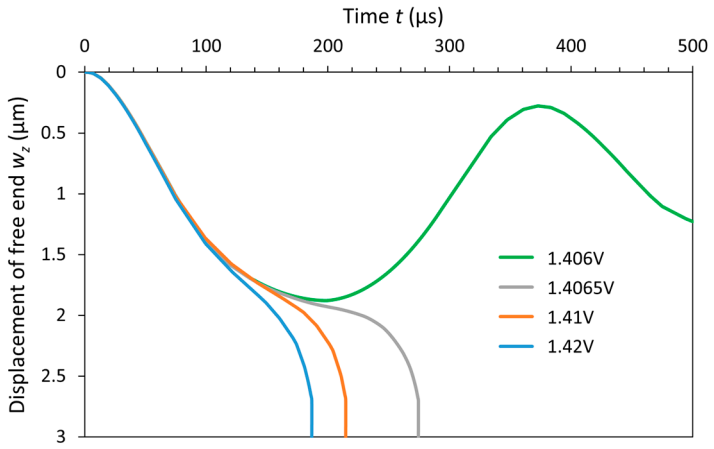


Figure 13. Temporal response of a longer Al MEMS cantilever tip for different applied voltages; l = 400 μm, b = 20 μm and h = 1 μm.

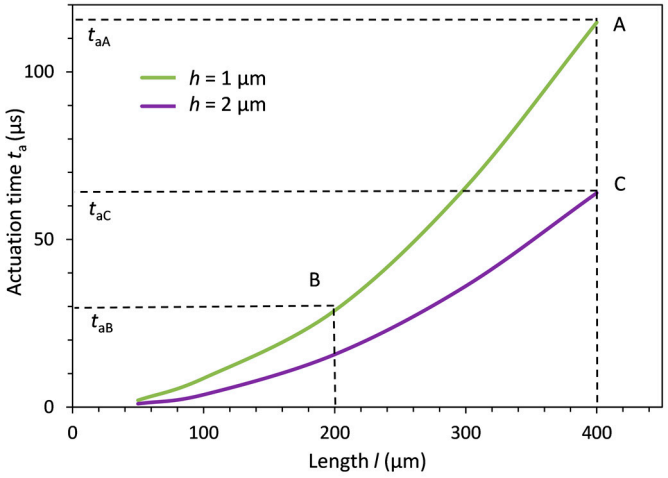


Figure 14. Variation of the actuation time t_a with length l and thickness h for Al MEMS cantilevers.

Figure 15 depicts the influence of variations in mass density ρ and Young's modulus E on actuation time t_a for the MEMS cantilevers with the parameters l = 100 μm, h = 1 μm, ρ = 5400–10800 kg/m^3 and E = 70–210 GPa. In three points D (ρ = 10800 kg/m^3, E = 70 GPa), E (ρ = 5400 kg/m^3, E = 70 GPa) and F (ρ = 10800 kg/m^3, E = 140 GPa) selected in Figure 15, the maximum actuation time t_{aD} occurs in point D. From point D to E, the mass density is halved, and the actuation time decreases by 24%. From point D to F, the Young's modulus is doubled and the actuation time reduces by 21%, which means the impact on actuation time from density and Young's modulus are relatively close to each other. Combining Figures 14 and 15, as the parameters l, h, ρ and E vary regularly (doubled and halved), the reduction ratios of t_a are 75%, 44%, 24% and 21%, respectively. The results show that the primary factors affecting actuation time are length, then thickness, and finally mass density and Young's modulus (in this sequence decreasing influence). This is because when the parameters h and E increase, while l and ρ decrease, the resonance frequency f_1 increases and the actuation time t_a is decreasing.

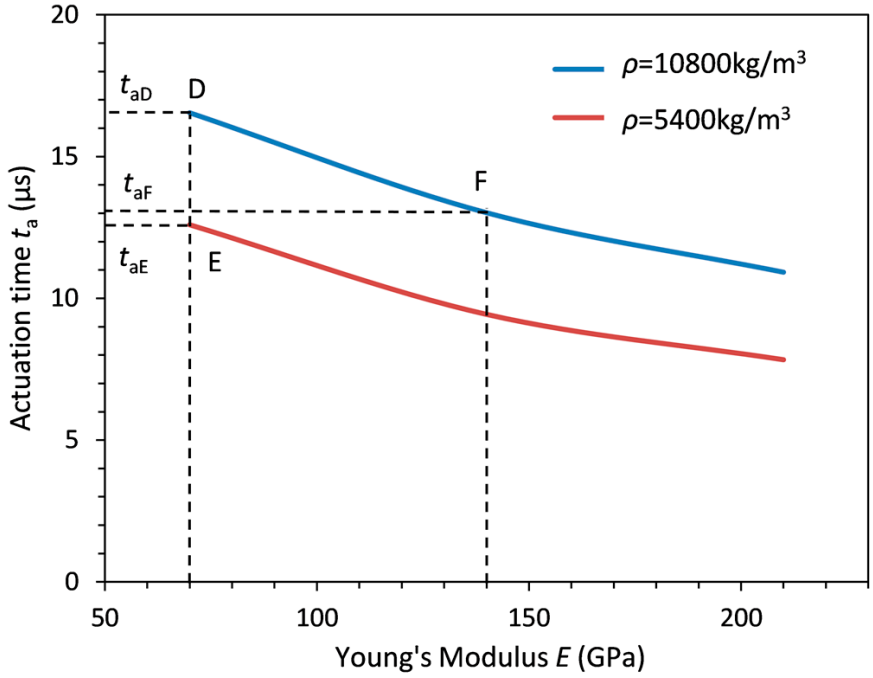


Figure 15. Variation of the actuation time t_a with mass density ρ and E for MEMS cantilevers (artificial materials).

The results are partly surprising concerning increasing thickness, since doubling the thickness doubles the mass. The negative influence of growing mass (inertia) is however overcompensated by the counter-running positive effect of growing thickness coming from much higher resonance frequencies.

4.4. Simulations on Pull-In and Actuation Time for Different Real Materials

Since pull-in voltage and actuation time are strongly dependent on material properties in a MEMS cantilever, it is interesting to plot the dynamic pull-in voltage V_{pi}' as a function of the actuation time t_a for MEMS cantilevers made of different metals, aluminum (Al), titanium (Ti), copper (Cu), nickel (Ni), silver (Ag), gold (Au), tungsten (W), tantalum (Ta), molybdenum (Mo) and chromium(Cr). The corresponding material properties are shown in Table 3.

Table 3. Properties of different metallic MEMS materials.

Material	Mass Density	Young's Modulus	Poisson Ratio
Aluminum (Al)	2700 kg/m^3	70 GPa	0.35
Titanium (Ti)	4506 kg/m^3	116 GPa	0.32
Copper (Cu)	8690 kg/m^3	120 GPa	0.34
Nickel (Ni)	8900 kg/m^3	219 GPa	0.31
Silver (Ag)	10,500 kg/m^3	83 GPa	0.37
Gold (Au)	19,300 kg/m^3	70 GPa	0.44
Tungsten (W)	19,350 kg/m^3	411 GPa	0.28
Tantalum (Ta)	16,690 kg/m^3	186 GPa	0.34
Molybdenum (Mo)	10,280 kg/m^3	329 GPa	0.31
Chromium (Cr)	7150 kg/m^3	279 GPa	0.21

The results are shown in Figure 16, and it is evident that the V_{pi}' and t_a have opposite tendencies, which means one value increases while the other decreases. If the curve is close to the vertical axis, this shows better high-speed performance of the MEMS cantilevers. If the curves are close to the horizontal axis, this shows better low-voltage performance of the MEMS cantilevers. Considering both V_{pi}' and t_a, it can be concluded that out of these considered metals, aluminum is the best for MEMS. For practical applications, low drive voltages and short actuation times are the most desirable goals, but it seems to be impossible to achieve both targets simultaneously. For application and research, it is important to consider the priorities and subsequently to make tailored optimum designs.

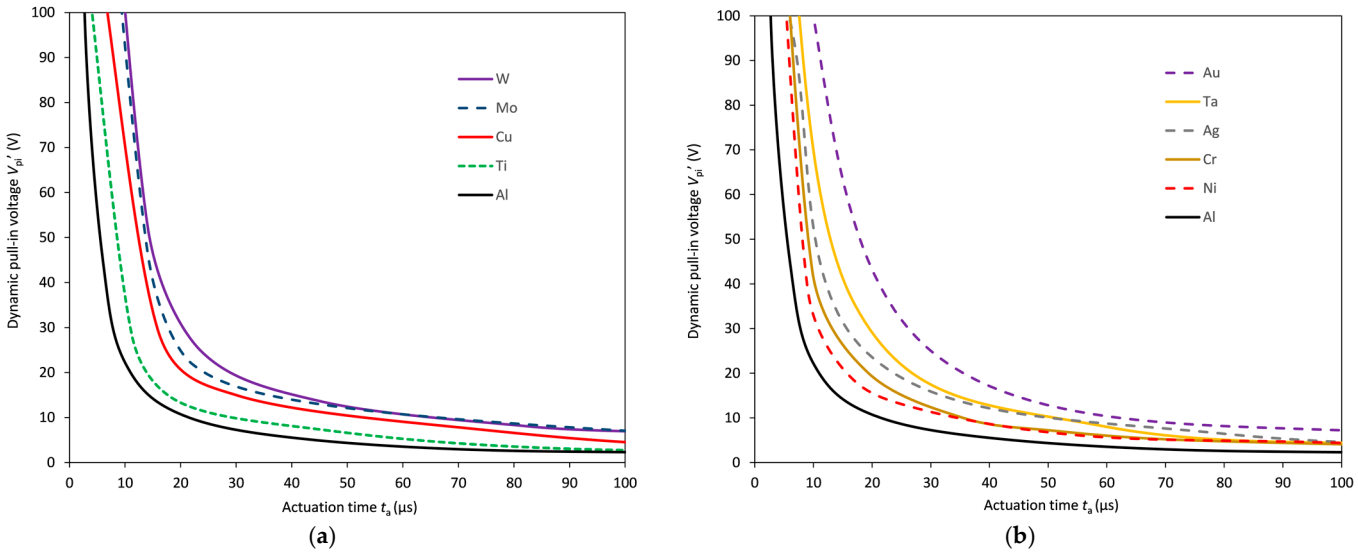


Figure 16. Relationships between dynamic pull-in voltage and actuation time of MEMS cantilevers made of (**a**) W, Cu, Ti, Mo and Al (**b**)Au, Cr, Ta, Ag, Ni and Al, Al appears as a reference in both sub-figures.

Finally, the calculated actuation times are related to experimental MEMS closing times. Table 4 includes the type and dimensions of the MEMS device, the material of the moving part of the MEMS device, the closing time and the possible application. Although no quantitative comparison is possible, a qualitative agreement with the findings of this paper is obtained. For example, the shortest closing time of 1 µs is obtained in our MEMS micro-shutters having l = 40 µm and the longest closing time of 62.3 ms is obtained for a long cantilever with l = 40 mm.

Due to the involved mechanical stress, the reported shutters and mirrors which have been fabricated are not easy to simulate. The stress in the thin layers modifies the elastic material properties. The material properties of very thin layers are often unknown and deviate from the values known for bulk materials. Deformations of thin stressed layers change the elastic properties additionally. This makes simulations of MEMS which include sub-layers (under stress) very challenging. Furthermore, an interdiffusion of material at interfaces, occurs and metallic surfaces are often covered by an unknown thin oxide layer. These altogether make a quantitative comparison between experiment and theory extremely challenging and sometimes nearly impossible. Thus, the qualitative agreement obtained in the last part is deemed acceptable. The metallic cantilever considered in this paper is a model structure to identify basic relations in nonlinear dynamics.

Table 4. Comparison of actuation times (here closing times) of MEMS shutters/mirrors/cantilevers. The type of the study is experimental or theoretical. The dimensions are given as long they are available from the literature. The dimensions are denoted as in this paper: length l, width b and thickness h. For the top electrode, which is moving, materials and dimensions are given. The type of the study is experimental or theoretical or both.

Ref.	Study Type	MEMS Type	MEMS Dimensions/µm	Moving Material	Closing Time/µs	Actuation Voltage/V	Application
[22–24]	Experiment	Curled shutter	l = 450–2400, b = 200–600, h = 0.5–1	Cu	100 200	80 180	Display and smart glass
[25,26]	Experiment	Flat mirror	l = 150, b = 400, h = 0.22	Al-Cr-Al	300	40	Light steering via smart glass
[33]	Experiment	Curled shutter	l = 600–1000, h = 1.25–1.6	Poly-Cr-Au-poly	18	180	Eyelid protection of sensors
[27,28]	Experiment	Curled shutter	l = 100–400, h = 0.1	Si-Cr and other metals	40	20	Light modulation via smart glass
[32]	Experiment	Curled triangularshutter	l = 1400, h = 0.3 + 0.35	Al/Mo/SiN_x	1000	30	Camera shutter
[34,35]	Experiment	Curled shutter	l = 200, b = 160, h = 0.1	Ti-Au	20	20	LED displays
[29]	Experiment	Curled shutter	l = 200, b = 30, h = 0.3	SiO_2-Al	3000	55	Light modulation via smart glass
This paper	Experiment	Curled shutter	l = 40, b = 2000 h = 0.185	Al-Cr-Al	1	100	Fast mechanical shutter for optics
[45]	Experiment	Cantilever	l = 140, b = 10–12, h = 2.2	$SiON_x$-Au	10.75 15	60 50	RF MEMS switch
[46]	Experiment	Cantilever	l = 10,000, b = 180, h = 50	Si	20,000	0.3	Fiber-optical switching device
[19]	Experiment	Cantilever	l = 650, b = 200, h = 0.3	Al	60	32	Audible frequency generator
[30]	Theory	Cantilever	l = 200, h = 0.1–0.6	Mo-Ta- SiN_x	<50	-	Display
[47]	Theory and Experiment	Cantilever	l = 40,000, b = 10,000, h = 50	Si	62,300	85	Electrostatic actuator
[48]	Theory and Experiment	Cantilever	l = 1500, b = 12, h = 60	Cu-Au	120	28	MEMS relays/switches
[49]	Theory and Experiment	Irregular Cantilever	l = 67, b = 42, h = 6	Au	2	55	MEMS electrostatic actuator

5. Discussion of Trends from Section 4 against Models Delivering Analytical Results

5.1. Comparison of Trends of Analytical Results for Parallel Plate MEMS Devices with Numerical Results from Section 4

Here, the results obtained by numerical simulations in Section 4 are qualitatively related to the analytic formula given in Sections 2 and 3 for a parallel plate MEMS actuator. Equation (4) in Section 2 reveals that the pull-in voltage V_{pi} is proportional to the root of the spring constant $\sqrt{k}$ and inversely proportional to the root of the area $\sqrt{A}$ of plates. Therefore, the V_{pi} of a parallel plate qualitatively increases with growing k and decreasing A.

The eigenfrequency f_{n} (described in Equation (5) of Section 3) for a parallel plate capacitor is proportional to the root of the spring constant $\sqrt{k}$ and inversely proportional to the root of the mass $\sqrt{m}$. Therefore, f_{n} increases with growing k and decreasing m. As mentioned before, the actuation time is reversely related to the frequency. Thus, the actuation time qualitatively increases with growing m and decreasing k.

Therefore, the simple formula of the parallel plate actuator can provide a preliminary qualitative tendency, even for such a simplified geometry (parallel plate actuation) compared to a cantilever actuator. For quantitative statements, numerical simulations (as performed in Section 4) are required.

5.2. Comparison of Trends of Analytical Results for MEMS Cantilevers with Numerical Results from Section 4

For a cantilever system, the spring constant can be roughly approximated by $kc = \frac{2Eb}{3}\left(\frac{h}{l}\right)^3$ [50]. Therefore, V_{pi} increases with growing E and h, and it increases with decreasing l. In the literature, the calculated pull-in voltage V_{pi} of cantilevers is reported to be proportional to $\sqrt{\frac{Eh^3}{l^4}}$ [51], which means that V_{pi} rises with growing E and h as well as with decreasing l. This trend is in agreement with the results obtained in Section 4. The results show that the primary factors affecting pull-in voltage are length, followed by thickness, and finally Young's modulus (showing decreasing influence in this sequence), which is consistent with the simulation results in Section 4.

Then, based on the eigenfrequency formula of cantilevers from Ref [52], f_{n} is proportional to $\sqrt{\frac{Eh^2}{\rho l^4}}$. Thus, f_{n} grows with increasing E and h as well as decreasing ρ and l. The actuation time is inversely proportional to the frequency, and the relation is also in agreement with our numerical simulations obtained in Section 4.

In many theoretical papers, the parameters in the results have been converted into reduced parameters (dimension-less). In order to enable a comparison with our results from Section 4, we reconverted the parameters, delivering the following: the actuation voltage V is proportional to $\sqrt{\frac{2d^3EI}{\varepsilon bl^4}}$ and the actuation time t_a is proportional to $\sqrt{\frac{\rho Sl^4}{EI}}$ [21,53]. For a cantilever, the area of the cross-section is $S = bh$, and the area moment of inertia is $I = \frac{bh^3}{12}$. Therefore, the pull-in voltage of the cantilever V_{pi} is proportional to $\sqrt{\frac{Eh^3}{l^4}}$, and the actuation time t_a is proportional to $\sqrt{\frac{\rho l^4}{Eh^2}}$. In addition, this trend is in agreement with the above-mentioned trends and in agreement with our numerical results from Section 4.

5.3. Proposed Optimization Concept

Figure 16 reveals that higher actuation voltages are required if cantilever thickness is increased. Thus, instead of reducing the actuation time, the opposite could also happen in practice due to non-idealities. Switching higher voltages results in longer electrical switching times, which is known from circuit design. That could reveal in practice that thicker cantilevers (requiring higher voltages) move slower in combination with real driving circuits, although simulations predict the opposite. Mobile sensors require in most cases that voltage sources from battery packs are used; therefore, the question of adequate voltage converters arises. The converters are only available in defined voltage steps and there are threshold values, making the converters considerably more bulky and more expensive. Thus, increasing the cantilever thickness could be beneficial, but it could also be contra-

productive, since electrical switching becomes slower, more expensive and bulkier in case larger voltages have to be modulated. Note that in many cases, size is superior to speed and the main goal is to reduce the actuation voltage in order to substantially miniaturize the driver circuit for mobile sensor applications in smart personal environments.

A possible approach for an optimization procedure is given here. Step 1: Identifying which degree of miniaturization (l, b) is still acceptable for the application, since the smaller the structure, the lower the required actuation voltage and the shorter the actuation times. Step 2: The thickness h is optimized. Step 3: For the chosen geometry (strongest acceptable miniaturization), the actuation time as a function of the pull-in voltage is calculated (Figure 16) for the envisaged metal heterostructure stack or metal stack with metal oxides on the top. Step 4: Finetuning of h and of the individual metal layer thicknesses is performed. Step 5: If no restrictions concerning the metals are existing, it is advisable to choose Al. Step 6: Several iterations involving steps 1–5 are performed to obtain planarization if it is required for the device performance. Step 7: Identifying which maximum voltage can be tolerated that still allows for envisaged economic and unbulky solutions for the drive circuits. This is related to the choice of adequate voltage converters. Choosing the maximum voltage is a trade-off between size (miniaturization), price and power consumption, and it has an influence on the smallest achievable switching time of the MEMS device. Step 8: Finally, some iterations involving all seven steps have to be performed.

Concerning the dynamical behavior, the performance of real MEMS devices is often deviating from theoretical model calculations due to strong non-linearities, non-idealities in the system, or by damping related to the geometry and the working environment.

6. Conclusions

The influences of material and geometrical properties on pull-in voltage and actuation speed have been studied. Comparing results obtained by numerical simulations with trends predicted from simple analytical formula, a similar tendency can be observed qualitatively. The formula can provide a qualitative tendency, even if only a simple parallel plate actuator is considered and compared to a more complex cantilever actuator. However, for quantitative statements, numerical simulations are required. Based on COMSOL Multiphysics® simulations, various results have been obtained for metallic cantilever actuators. If a short actuation time is the goal, the most important dependencies are:

- Thicker cantilevers are acting faster;
- Shorter cantilevers are acting faster;
- Cantilevers with larger E are acting faster;
- Cantilevers with smaller ρ ratio are acting faster; and
- Higher step function voltages make the actuation faster.

However, if the cantilever thickness is increased, higher actuation voltages are also required, which could be contra-productive, since electrical switching becomes slower with larger actuation voltages.

Our simulations reveal that reducing actuation time and actuation voltage cannot be obtained at the same time. However, optimizing the material is found to be efficient. Different metals such as Au, Ag, Cu, Ti, Ni, Al, W, Cr, Ta, and Mo as well as artificial metals are studied and compared. Aluminum is found to be an ideal material concerning the improvement with respect to smaller pull-in voltages and shorter actuation times.

The calculated actuation times are found to be in the same order of magnitude as experimental data from the literature. The trends obtained from numerical simulations are also in agreement with the trends from analytical formula for MEMS cantilevers and MEMS parallel plate actuators.

Author Contributions: Conceptualization, H.H., Q.L. and X.Y.; Methodology, H.H., P.K. and X.Y.; Validation, X.Y., P.K., E.K. and H.H.; Formal Analysis, X.Y., P.K., E.K. and H.H.; Investigation, X.Y. M.S. and S.L.; Writing—Original Draft Preparation, X.Y., H.H.; Writing—Review and Editing, all

authors; Visualization, X.Y. and H.H.; Funding Acquisition, H.H. and Q.L. All authors have read and agreed to the published version of the manuscript.

Funding: This research was funded by Deutscher Akademischer Austauschdienst (DAAD): DAAD STIBET Degree Completion Support 2022 (using corresponding author's name but no number); Deutsche Forschungsgemeinschaft (DFG):(grant number: Nos Hi 763/21-1 and Hi 763/19-1); Deutsche Bundesstiftung Umwelt (DBU):(grant number: Nos. AZ23717, AZ20012/189, and AZ35501); and Bundesministerium für Bildung und Forschung (BMBF):(grant number: Nos. 13N14517 and 13N15740).

Institutional Review Board Statement: Not applicable.

Informed Consent Statement: Not applicable.

Data Availability Statement: Not applicable.

Acknowledgments: The authors would like to thank R. Donatiello, I. U. Haq Emal, B. Elsaka, M. S. Q. Iskandar, K. Hasan, D. Löber, S. Nazemroaya, S. Liebermann, S. Baby, M. Qasim, G. Xu, A. Friedrichsen, J. Krumpholz, H. Wilke, N. Körte, and T. Thomas for fruitful discussions and technological support; as well as DAAD STIBET Degree Completion Support 2022, DFG (Nos Hi 763/21-1 and Hi 763/19-1), DBU (Nos. AZ23717, AZ20012/189, and AZ35501), and BMBF (Nos. 13N14517 and 13N15740) for financial support. The author X. Y. acknowledges gratefully the support by the Ph.D. scholarship of DAAD and University of Kassel.

Conflicts of Interest: The authors declare no conflict of interest.

References

1. Bogue, R. Recent developments in MEMS sensors: A review of applications, markets and technologies. *Sens. Rev.* **2013**, *33*, 300–304. [CrossRef]
2. Lang, H.P.; Hegner, M.; Gerber, C. Cantilever array sensors. *Mater. Today* **2005**, *8*, 30–36. [CrossRef]
3. Majumder, S.; McGruer, N.E.; Adams, G.G.; Zavracky, P.M.; Morrison, R.H.; Krim, J. Study of contacts in an electrostatically actuated microswitch. *Sens. Actuators A Phys.* **2001**, *93*, 19–26. [CrossRef]
4. McCarthy, B.; Adams, G.G.; McGruer, N.E.; Potter, D. A dynamic model, including contact bounce, of an electrostatically actuated microswitch. *J. Microelectromechanical Syst.* **2002**, *11*, 276–283. [CrossRef]
5. Verma, G.; Mondal, K.; Gupta, A. Si-based MEMS resonant sensor: A review from microfabrication perspective. *Microelectron. J.* **2021**, *118*, 105210. [CrossRef]
6. Hung, E.S.; Senturia, S.D. Extending the travel range of analog-tuned electrostatic actuators. *J. Microelectromechanical Syst.* **1999**, *8*, 497–505. [CrossRef]
7. Zhang, W.-M.; Yan, H.; Peng, Z.-K.; Meng, G. Electrostatic pull-in instability in MEMS/NEMS: A review. *Sens. Actuators A Phys.* **2014**, *214*, 187–218. [CrossRef]
8. Do, C.; Lishchynska, M.; Delaney, K.; Hill, M. Generalized closed-form models for pull-in analysis of micro cantilever beams subjected to partial electrostatic load. *Sens. Actuators A Phys.* **2012**, *185*, 109–116. [CrossRef]
9. Sharma, J.; DasGupta, A. Effect of stress on the pull-in voltage of membranes for MEMS application. *J. Micromechanics Microengineering* **2009**, *19*, 115021. [CrossRef]
10. Chu, C.-H.; Shih, W.-P.; Chung, S.-Y.; Tsai, H.-C.; Shing, T.-K.; Chang, P.-Z. A low actuation voltage electrostatic actuator for RF MEMS switch applications. *J. Micromechanics Microengineering* **2007**, *17*, 1649–1656. [CrossRef]
11. Ghayesh, M.H.; Farokhi, H.; Amabili, M. Nonlinear behaviour of electrically actuated MEMS resonators. *Int. J. Eng. Sci.* **2013**, *71*, 137–155. [CrossRef]
12. Chen, R.T.; Nguyen, H.; Wu, M.C. A high-speed low-voltage stress-induced micromachined 2 x 2 optical switch. *IEEE Photonics Technol. Lett.* **1999**, *11*, 1396–1398. [CrossRef]
13. Dai, H.L.; Wang, L. Size-dependent pull-in voltage and nonlinear dynamics of electrically actuated microcantilever-based MEMS: A full nonlinear analysis. *Commun. Nonlinear Sci. Numer. Simul.* **2017**, *46*, 116–125. [CrossRef]
14. Liu, X.F.; Yan, G.G.; Shen, Z.W.; Wen, Z.X.; Chen, J.; He, Y.W.; Zhao, W.S.; Wang, L.; Guan, M.; Zhang, F.; et al. Theoretical Calculation and Simulation for Microcantilevers Based on SiC Epitaxial Layers. *Mater. Sci. Forum* **2019**, *954*, 26–30. [CrossRef]
15. Siddaiah, N.; Manjusree, B.; Aditya, A.L.G.N.; Reddy, D.V.R.K. Design Simulation and Analysis of U-Shaped and Rectangular MEMS Based Triple Coupled Cantilevers. *J. Sci. Ind. Res.* **2017**, *76*, 235–238.
16. Tuma, J.; Skutova, J. Simulation of active vibration control of the cantilever beam. In Proceedings of the 13th International Carpathian Control Conference (ICCC), High Tatras, Slovakia, 28–31 May 2012; pp. 744–747.
17. Sánchez-Fraga, R.; Ponce-Ponce, V.H.; Mendoza-Acevedo, S.; Villa-Vargas, L.A.; Estrada-Vázquez, H. Design and simulation of mass sensors based on horizontally actuated silicon cantilevers. *Microelectron. Eng.* **2014**, *119*, 83–88. [CrossRef]
18. Xu, F.; Wei, Y.; Bian, S.; Wang, H.; Chen, D.R.; Kong, D. Simulation-Based Design and Optimization of Rectangular Micro-Cantilever-Based Aerosols Mass Sensor. *Sensor* **2020**, *20*, 626. [CrossRef]

19. Arya, S.; Khan, S.; Lehana, P. Design and fabrication of electrostatic micro-cantilever array as audible frequency generator. *J. Electrost.* **2015**, *76*, 145–151. [CrossRef]
20. Zega, V.; Martinelli, L.; Casati, R.; Zappa, E.; Langfelder, G.; Cigada, A.; Corigliano, A. A 3D Printed Ti6Al4V Alloy Uniaxial Capacitive Accelerometer. *IEEE Sens. J.* **2021**, *21*, 19640–19646. [CrossRef]
21. Sharma, A.K.; Godara, R.K.; Joglekar, M.M. Static and DC dynamic pull-in analysis of curled microcantilevers with a compliant support. *Microsyst. Technol.* **2018**, *25*, 965–975. [CrossRef]
22. Pizzi, M.; Koniachkine, V.; Bassino, E.; Sinesi, S.; Perlo, P.P. Electrostatic microshutters-micromirrors array for light modulation systems. In Proceedings of the SPIE, Miniaturized Systems with Micro-optics and MEMS, Santa Clara, CA, USA, 20–22 September 1999; pp. 164–171.
23. Roux, P.; Woirgard, E.; Pizzi, M.; Martiis, O.D.; Koniachkine, V. Fem modelling of an electro-optical micro-shutter. *Sens. Actuators A Phys.* **2005**, *119*, 1–7. [CrossRef]
24. Pizzi, M.; Koniachkine, V.; Nieri, M.; Sinesi, S.; Perlo, P. Electrostatically driven film light modulators for display applications. *Microsyst. Technol.* **2003**, *10*, 17–21. [CrossRef]
25. Hillmer, H.; Al-Qargholi, B.; Khan, M.M.; Worapattrakul, N.; Wilke, H.; Woidt, C.; Tatzel, A. Optical MEMS-based micromirror arrays for active light steering in smart windows. *Jpn. J. Appl. Phys.* **2018**, *57*, 08PA07. [CrossRef]
26. Hillmer, H.H.; Iskhandar, M.S.Q.; Hasan, M.K.; Akhundzada, S.; Al-Qargholi, B.; Tatzel, A. MOEMS micromirror arrays in smart windows for daylight steering. *J. Opt. Microsyst.* **2021**, *1*, 014502. [CrossRef]
27. Lamontagne, B.; Barrios, P.; Py, C.; Nikumb, S. The next generation of switchable glass: The micro-blinds. In Proceedings of the Glass Performance Days, Tampere, Finland, 11–12 June 2009; pp. 637–639.
28. Lamontagne, B.; Fong, N.R.; Song, I.-H.; Ma, P.; Barrios, P.; Poitras, D. Review of microshutters for switchable glass. *J. Micro/Nanolithography MEMS MOEMS* **2019**, *18*, 040901. [CrossRef]
29. Mori, K.; Misawa, K.; Ihida, S.; Takahashi, T.; Fujita, H.; Toshiyoshi, H. A MEMS Electrostatic Roll-Up Window Shade Array for House Energy Management System. *IEEE Photonics Technol. Lett.* **2016**, *28*, 593–596. [CrossRef]
30. Schalberger, P.; Al Nusayer, S.A.; Raichle, C. 54-1: Parallel Fabrication for Integration of Electronic and Microelectromechanical Systems. *SID Symp. Dig. Technol. Pap.* **2016**, *47*, 731–734. [CrossRef]
31. Akhundzada, S.; Yang, X.; Fiedler, J.; Käkel, E.; Al-Qargholi, B.; Buhmann, S.; Ehresmann, A.; Hillmer, H. A novel approach to construct self-assembled 3D MEMS arrays. *Microsyst. Technol.* **2022**, *28*, 2139–2148. [CrossRef]
32. Kim, C.-H.; Hong, S. Study on the reliability of the mechanical shutter utilizing roll actuators. In Proceedings of the 2011 IEEE 24th International Conference on Micro Electro Mechanical Systems, Cancun, Mexico, 23–27 January 2011.
33. Goodwin-Johansson, S.; Davidson, M.; Dausch, D.; Holloway, P.H.; McGuire, G. Reduced voltage artificial eyelid for protection of optical sensors. In Proceedings of the Smart Structures and Materials 2002: Electroactive Polymer Actuators and Devices (EAPAD), San Diego, CA, USA, 18–21 March 2002; pp. 451–458.
34. Lim, K.-S.; Chung, J.; Yoo, S.; Yoon, J.-B. P-67: Wide Bandwidth Reflective Microshutter Blind Panel for Transparent Organic Light-Emitting Diode Display. *SID Symp. Dig. Technol. Pap.* **2016**, *47*, 1389–1391. [CrossRef]
35. Lee, K.-H.; Chang, J.; Yoon, J.-B. High performance microshutter device with space-division modulation. *J. Micromechanics Microengineering* **2010**, *20*, 075030. [CrossRef]
36. Nielson, G.N.; Barbastathis, G. Dynamic Pull-In of Parallel-Plate and Torsional Electrostatic MEMS Actuators. *J. Microelectromechanical Syst.* **2006**, *15*, 811–821. [CrossRef]
37. Dorf, R.C.; Bishop, R.H. *Modern Control Systems*, 12th ed.; Pearson Prentice Hall: Madrid, Spain, 2008; pp. 308–314.
38. COMSOL Multiphysics®MEMS Module: Electrostatically Actuated Cantilever. Available online: https://www.comsol.com/model/electrostatically-actuated-cantilever-444 (accessed on 1 October 2022).
39. COMSOL Multiphysics®Documentation: Rayleigh Damping. Available online: https://doc.comsol.com/5.6/doc/com.comsol.help.sme/sme_ug_modeling.05.086.html#618126 (accessed on 12 December 2022).
40. Colakoglu, M. Factors effecting internal damping in aluminum. *J. Theor. Appl. Mech.* **2004**, *42*, 95–105.
41. Krylov, S.; Maimon, R. Pull-in Dynamics of an Elastic Beam Actuated by Continuously Distributed Electrostatic Force. *J. Vib. Acoust.* **2004**, *126*, 332–342. [CrossRef]
42. Ashby, M.F. *Materials Selection in Mechanical Design*, 4th ed.; Elsevier: Burlington, MA, USA, 2011; pp. 59–62.
43. Krylov, S. Lyapunov exponents as a criterion for the dynamic pull-in instability of electrostatically actuated microstructures. *Int. J. Non-Linear Mech.* **2007**, *42*, 626–642. [CrossRef]
44. Chaterjee, S.; Pohit, G. A large deflection model for the pull-in analysis of electrostatically actuated microcantilever beams. *J. Sound Vib.* **2009**, *322*, 969–986. [CrossRef]
45. Liu, L. High Performance RF MEMS Series Contact Switch—Design and Simulations. In Proceedings of the 2007 Proceedings 57th Electronic Components and Technology Conference, Sparks, NV, USA, 29 May–1 June 2007; pp. 158–164.
46. Matsuura, T.; Fukami, T.; Chabloz, M.; Sakai, Y.; Izuo, S.-i.; Uemura, A.; Kaneko, S.-i.; Tsutsumi, K.; Hamanaka, K. Silicon micro optical switching device with an electromagnetically operated cantilever. *Sens. Actuators A Phys.* **2000**, *83*, 220–224. [CrossRef]
47. Castañer, L.; Rodríguez, A.; Pons, J.; Senturia, S.D. Pull-in time–energy product of electrostatic actuators: Comparison of experiments with simulation. *Sens. Actuators A Phys.* **2000**, *83*, 263–269. [CrossRef]
48. Bian, W.; Zhao, J.; You, Z. Low voltage, high speed and small area in-plane MEMS switch. *J. Micromechanics Microengineering* **2019**, *29*, 065014. [CrossRef]

49. Do, C.; Lishchynska, M.; Cychowski, M.; Delaney, K.; Hill, M. Energy-Based Approach to Adaptive Pulse Shaping for Control of RF-MEMS DC-Contact Switches. *J. Microelectromechanical Syst.* **2012**, *21*, 1382–1391. [CrossRef]
50. Rebeiz, G.M. *RF MEMS Theory, Design, and Technology*; John Wiley & Sons: Hoboken, NJ, USA, 2004; pp. 31–32.
51. Chowdhury, S.; Ahmadi, M.; Miller, W.C. A closed-form model for the pull-in voltage of electrostatically actuated cantilever beams. *J. Micromechanics Microengineering* **2005**, *15*, 756–763. [CrossRef]
52. Gatti, P.L. *Applied Structural and Mechanical Vibrations*; CRC Press: Boca Raton, FL, USA, 1999.
53. Joglekar, M.M.; Pawaskar, D.N. Estimation of oscillation period/switching time for electrostatically actuated microbeam type switches. *Int. J. Mech. Sci.* **2011**, *53*, 116–125. [CrossRef]

Disclaimer/Publisher's Note: The statements, opinions and data contained in all publications are solely those of the individual author(s) and contributor(s) and not of MDPI and/or the editor(s). MDPI and/or the editor(s) disclaim responsibility for any injury to people or property resulting from any ideas, methods, instructions or products referred to in the content.